Beam deflection measurement of time and polarization resolved ultrafast nonlinear refraction

Manuel R. Ferdinandus,[1] Honghua Hu,[1] Matthew Reichert,[1] David J. Hagan,[1,2] and Eric W. Van Stryland[1,2,*]

[1]*CREOL, The College of Optics and Photonics, University of Central Florida, Orlando, Florida 32816, USA*

[2]*Department of Physics, University of Central Florida, Orlando, Florida 32816, USA*

**Corresponding author: ewvs@creol.ucf.edu*

Received June 6, 2013; accepted July 7, 2013;
posted August 8, 2013 (Doc. ID 191861); published September 5, 2013

We modify the well-known photothermal beam deflection technique to study ultrafast nonlinearities. Using phase-sensitive detection we directly measure the temporal and polarization dynamics of nonlinear refraction (NLR) with sensitivity to optically induced phase changes of approximately $\lambda/20,000$. We use the relative polarization dependence of excitation and probe to separate the isotropic and reorientational components of the NLR.

OCIS codes: (190.4400) Nonlinear optics, materials; (190.3270) Kerr effect.
http://dx.doi.org/10.1364/OL.38.003518

Knowledge of the magnitude and temporal response of the nonlinear refraction (NLR) and absorption of materials allows for understanding of the physical mechanisms underlying the nonlinear response. Various experimental techniques are devoted to measuring the nonlinear optical (NLO), response. For example, Z-scan [1] provides the refractive and absorptive components of the NLO response, excite-probe [2] provides the temporal response of the absorption, and optical Kerr experiments (OKE) [3,4] give the temporal response of the induced birefringence.

We apply the previously developed technique of photothermal beam deflection, used extensively to measure weak linear absorption [5,6], to measure the magnitude, sign, and temporal response of the NLR of materials. In photothermal beam deflection, a strong CW excitation beam is overlapped with a weak probe beam that is slightly shifted in space so that the index gradient induced by the excitation is maximum. This index gradient deflects the probe beam, whose deflection is measured by a segmented bi-cell detector that determines the beam position.

Our application of the beam deflection method measures the absolute magnitude, sign, and temporal dynamics of the NLR with high sensitivity and with the flexibility to resolve its tensor elements using different combinations of polarization of light. As an excite-probe technique utilizing cross-phase modulation [7], a temporal delay, τ_d, between excitation and probe resolves the dynamics of the nonlinear response, and the ultrafast nonlinearities may be distinguished from slower effects. By independently varying the wavelength or polarization of the two beams, it can also be used to study the dispersion of different tensor elements of the nonlinear susceptibility.

This technique is much easier to implement than the two-color Z-scan [8], which requires careful beam alignment to ensure collinearity, the derivative method of cross-induced beam deformation [9,10], or time division/spectral interferometry techniques, [11,12], which are more sensitive to environmental perturbations. It is also more flexible than OKE, which measures only the induced birefringence.

Position sensitive bi-cell detectors were previously used in Kerr lens measurements to detect the spot size change of the probe beam on the detector, while the probe and excitation beams were aligned concentrically at the sample. [13,14] This was used to characterize relative temporal dynamics without measuring their absolute magnitude.

Assuming no nonlinear absorption (NLA) is present and the excitation spot size is much larger than the probe ($>3\times$) beam at the sample plane, we can approximate the index gradient to be linear in the y direction and nearly constant in the x direction (see Fig. 1). Furthermore, we work in the thin sample approximation, i.e., the sample thickness $L < z_0$, where z_0 is the Rayleigh range, and the nonlinear phase shift, defined as $\Delta\Phi = k_0 \Delta n L$, is small (i.e., $\Delta\Phi \ll 1$). For the materials used here the depletion of the excitation beam is also negligible. Thus, we can approximate the index gradient induced by the excitation as a thin prism that deflects the beam by a small deflection angle θ [15,16]:

$$\theta(x, y, t) = \int_{z=0}^{L} \nabla n_p(x, y, t) \cdot \mathrm{d}z, \tag{1}$$

where $n_p(x, y, t)$ is the spatially and temporally varying index of the material as seen by the probe. If the angle between the beams is small (2° in our case) the gradient seen by the probe is nearly constant so that $\theta(x, y, t) = \nabla n_p(x, y, t) L$.

For the general case of NLR induced by a spatially Gaussian excitation beam,

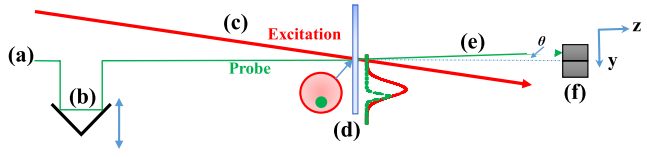

Fig. 1. Beam deflection schematic. (a) Probe beam, (b) delay line, (c) excitation beam, (d) sample and the overlap between excitation and probe spot, (e) deflected probe beam for positive nonlinearity, and (f) quad cell detector.

$$\Delta n_p(x,y,t) = \Delta n_p(t)\exp\left(\frac{-2(x^2+y^2)}{w_e^2}\right), \quad (2)$$

where $\Delta n_p(t)$ is the induced index change given by the convolution of the material response and the excitation irradiance, and w_e is the spot size (HW1/e^2M) of the excitation beam. For $\chi^{(3)}$ effects, this index change is proportional to the irradiance.

The maximum deflection occurs when the probe is placed at $x = 0$ and $y = w_e/2$, so that

$$\theta(t) = \frac{2L}{w_e\sqrt{e}}\Delta n_p(t). \quad (3)$$

Next, we Gaussian propagate the deflected probe to the quad cell. The instantaneous irradiance at the detector, located at a distance, d, behind the sample, is

$$I_p(x,y,t-\tau_d,d) = I_{p,0}(d) \cdot \exp\left(-\frac{2\pi^2 w_{p,0}^2((y-\Delta S(t))^2+x^2)}{d^2\lambda_p^2} - \frac{(t-\tau_d)^2}{\tau_p^2}\right), \quad (4)$$

where $I_{p,0}(d)$ is the peak irradiance at the detector, λ_p is the wavelength of the probe, $w_{p,0}$ is the beam waist (HW1/e^2M) of the probe, τ_p is the pulse duration of the probe (HW1/eM), and $\Delta S(t) = d{\cdot}\theta(t)$ (for small deflection angles $\theta(t)$) is the lateral translation of the probe on the detector. Integrating over the x–y plane gives us the difference in probe power ΔP_p incident on the left and right sides of the bi-cell detector:

$$\Delta P_p(t-\tau_d) \cong P_p(t-\tau_d)\cdot k_{0,p}L\sqrt{\frac{2}{e}}\frac{w_{p,0}}{w_e}\frac{2}{\sqrt{\pi}}\Delta n_p(t), \quad (5)$$

where $P_p(t-\tau_d)$ is the power of the probe on the detector, $k_{0,p} = 2\pi/\lambda_p$, and here we have used the approximation $erf(x) \approx 2x/\sqrt{\pi}$ for small x.

We next integrate over time to determine the normalized signal on the bi-cell detector by

$$\frac{\Delta E_p(\tau_d)}{E_p} = \int_{-\infty}^{\infty}\Delta P_p(t-\tau_d)\mathrm{d}t \Big/ \int_{-\infty}^{\infty}P_p(t-\tau_d)\mathrm{d}t = k_{0,p}L\sqrt{\frac{2}{e}}\frac{w_{p,0}}{w_e}\frac{2}{\sqrt{\pi}}\langle\Delta n_p\rangle, \quad (6)$$

where $\langle\Delta n_p\rangle$ is the time averaged index change over the temporal profile of the probe, and ΔE is the energy difference between the left and right segments. This expression is accurate for $\Delta E_p(\tau_d)/E_p < 20\%$, which can be controlled by adjusting the excitation pulse energy, E_p. Note that the sign of $\Delta E_p(\tau_d)/E_p$ gives the sign of the NLR.

For bound-electronic nonlinearities, the index change instantaneously follows the excitation irradiance, and $\langle\Delta n_p\rangle$ can be expressed as

$$\langle\Delta n_p\rangle = 2n_2(\lambda_p,\lambda_e)\int_{-\infty}^{\infty}I_p(t-\tau_d)I_e(t)\mathrm{d}t \Big/ \int_{-\infty}^{\infty}I_p(t-\tau_d)\mathrm{d}t, \quad (7)$$

where $\Delta n_p(t) = 2n_2(\lambda_p;\lambda_e)\cdot I_e(t)$, $I_e(t)$ is the temporal profile of the excitation irradiance, and $n_2(\lambda_p;\lambda_e)$ is the nondegenerate bound-electronic nonlinear refractive index. Therefore, $\Delta E_p(\tau_d)/E_p$ is essentially the cross correlation between excitation and probe pulses, if the group velocity mismatch (GVM) between excitation and probe pulses is negligible. For temporal Gaussian pulses, the relation between peak $\Delta E_p(\tau_d)/E_p$ and $n_2(\lambda_p;\lambda_e)$ can be analytically derived from Eqs. (6) and (7) as

$$\frac{\Delta E_p}{E_p} = k_{0,p}L\sqrt{\frac{2}{e}}\frac{w_{p,0}}{w_e}\frac{4n_2(\lambda_p,\lambda_e)I_{e,0}}{\sqrt{\pi}\sqrt{1+\tau_p^2/\tau_e^2}}, \quad (8)$$

where $I_{e,0}$ is the peak on-axis irradiance of the excitation and τ_e is the excitation pulse duration (HW1/eM). Note that the signal is proportional to the ratio $w_{p,0}/w_e$. This is due to a smaller w_e yielding an increase in irradiance, while the large $w_{p,0}$ yields a smaller spot on the detector, thus a larger signal for a given deflection.

For many materials the total refractive index change may be due to a combination of instantaneous (i.e., bound-electronic), and noninstantaneous (e.g., induced by nuclear movement) responses [17]. Then $\langle\Delta n_p\rangle$ and thus $\Delta E_p(\tau_d)/E_p$ is proportional to the convolution between the response function of the material and the cross correlation of the excitation and probe pulses [18].

The experimental apparatus is a simple modification to a standard excite-probe setup [2] [Fig. 1(a)]. The excitation pulse was generated from a Ti:sapphire amplified system (Clark-MXR CPA 2010) producing ~1 mJ, 150–250 fs (FWHM) pulses at 780 nm operating at a 1 kHz repetition rate. The probe pulse was set at 650 nm, generated from the spatially filtered output of an optical parametric generator/amplifier (OPG/OPA, Light Conversion TOPAS-C) pumped by the same laser system. The spot size (determined by knife-edge scans) of the excitation, w_e, was set to 4–5 times that of the beam waist of the probe, $w_{p,0}$. The probe was shifted from the peak of the excitation so that the probe experienced a nearly uniform maximized index gradient, as shown in Fig. 1(d). This was accomplished by shifting the excitation until the maximum deflection signal was achieved. The beam deflection was observed using an OSI QD50-0-SD quad-segmented photodiode, which can simultaneously measure E_p and $\Delta E_p(\tau_d)$. We detected $\Delta E_p(\tau_d)$ by modulating the excitation at 286 Hz by a mechanical optical chopper synchronized with the excitation repetition rate. To monitor energy fluctuations of the probe pulses, a second lock-in amplifier was used to record E_p.

To demonstrate this technique, measurements were performed on a 1 mm thick fused silica slide, as shown in Fig. 2. We observed a peak $\langle\Delta n_{p,\mathrm{co}}\rangle = 1.58\times10^{-5}$ with excitation and probe copolarized, and peak $\langle\Delta n_{p,\mathrm{cross}}\rangle = 0.51\times10^{-5}$ with the beams cross-polarized under the same peak excitation irradiance ($I_{e,0} = 51$ GW/cm^2). For isotropic media where the bound electronic nonlinearity dominates, the ratio $\Delta n_{p,\mathrm{co}}/\Delta n_{p,\mathrm{cross}}$, proportional to $\chi^{(3)}_{1111}/\chi^{(3)}_{1122}$, is 3, and the temporal response

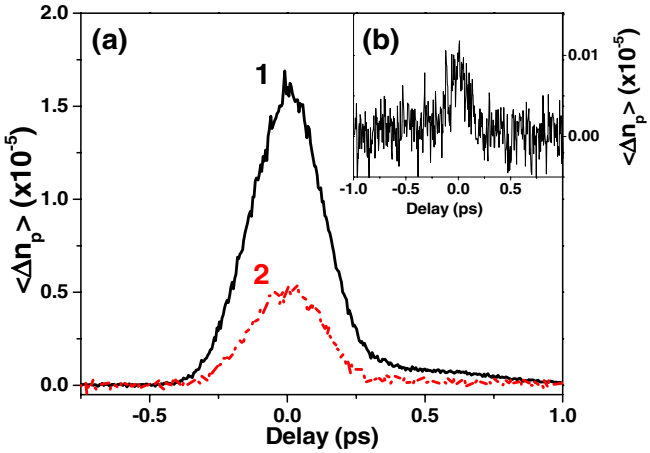

Fig. 2. Averaged index change $\langle \Delta n_p \rangle$ as a function of delay τ_d in fused silica for copolarized (1) and cross-polarized cases (2), with $L = 1$ mm, $\lambda_e = 780$ nm, $\lambda_p = 650$ nm, $w_e = 170$ μm, $w_{p,0} = 35$ μm, $\tau_e = 241$ fs, and $\tau_p = 170$ fs. (a) $I_{e,0} = 51$ GW/cm^2 and (b) inset, $I_{e,0} = 0.35$ GW/cm^2.

follows the cross-correlation traces between excitation and probe pulses [19]. Here we measure a ratio of 3.05 ± 0.28. The n_2 estimated from Fig. 2 in the copolarized case is $0.2 \pm 0.05 \times 10^{-15}$ cm^2/W, as compared to the literature value of 0.3×10^{-15} cm^2/W [20]. By reducing the irradiance to 0.35 GW/cm^2, as shown in Fig. 2(b), we could determine our minimum detectable $\langle \Delta n_p \rangle_{\min} = 3.0 \times 10^{-8}$, corresponding to a minimum induced peak phase change of $\sim \lambda/20,000$.

In order to study the temporal response of the noninstantaneous components to NLR originating from the nuclear response of the material, we performed the experiment on neat carbon disulfide, CS_2, in a 1 mm fused silica cell. The excitation pulse was generated by a multistage Ti:sapphire chirped pulse amplifier system (Coherent Legend Duo+) with 12 mJ output energy at a repetition rate of 1 kHz. The pulse width was 50 fs (FWHM), determined by autocorrelation. A small portion of the excitation pulse (<1%) was focused in a 1 cm water cell to generate a white-light continuum. 650 nm was selected as the probe pulse by a narrow bandpass filter. The probe pulse width was 155 fs (FWHM), determined by the beam deflection experiment (i.e., cross-correlation of excitation and probe pulses) performed with fused silica. To investigate the polarization dependence of the nonlinear response, we inserted a half-wave plate in the probe to rotate its polarization with respect to the excitation.

The induced refractive index change $\Delta n(\varphi)$, can be described by the index ellipsoid equation [19] in birefringent media (here the birefringence is induced by the excitation). For small index changes this equation reduces to

$$\Delta n(\varphi) = \Delta n_x \cos^2(\varphi) + \Delta n_y \sin^2(\varphi), \tag{9}$$

where the excitation is oriented along the x direction, and Δn_x and Δn_y are the refractive index changes for copolarized ($\varphi = 0°$), and cross-polarized ($\varphi = 90°$) cases.

The ratio $\Delta n_x/\Delta n_y$ is determined by the tensor elements of "$\chi^{(3)}$" (instantaneous or cascaded $\chi^{(1)}{:}\chi^{(1)}$, e.g., reorientational processes). It is known that in an isotropic medium $\Delta n_x/\Delta n_y = 3$ [19]; however, for CS_2 the excitation beam creates an anisotropy due to molecular reorientation, which leads to $\Delta n_x/\Delta n_y = -2$ [19]. For neat CS_2, where the nonlinearity is dominated by isotropic and reorientational-like nonlinearities [8], Eq. (9) can be written as

$$\Delta n(\varphi) = \Delta n_{\text{iso}}[\cos^2(\varphi) + \frac{1}{3}\sin^2(\varphi)] + \Delta n_{\text{re}}[\cos^2(\varphi) - \frac{1}{2}\sin^2(\varphi)], \tag{10}$$

where Δn_{iso}, and Δn_{re} are the refractive index changes along the excitation polarization originating from isotropic and reorientational nonlinearities, respectively [9].

We use three different implementations of Eq. (10) corresponding to $\varphi = 0°$, $90°$, and $54.7°$, respectively, where Δn is given by

$$\Delta n_{\text{co}} = \Delta n_{\text{iso}} + \Delta n_{\text{re}} \quad (\varphi = 0°), \tag{11a}$$

$$\Delta n_{\text{cross}} = \frac{1}{3}\Delta n_{\text{iso}} - \frac{1}{2}\Delta n_{\text{re}} \quad (\varphi = 90°), \tag{11b}$$

$$\Delta n_{\text{magic}} = \frac{5}{9}\Delta n_{\text{iso}} \quad (\varphi = 54.7°). \tag{11c}$$

Note, at the "magic angle" (i.e., $\varphi = 54.7°$), Δn induced by reorientational nonlinearities is zero, leaving only the isotropic term [10]. Figure 3 shows $\langle \Delta n_p \rangle$ as obtained from Eq. (6) as a function of temporal delay between excitation and probe for CS_2. Here the noninstantaneous response time is much longer than the cross-correlation width. In the copolarized ($\varphi = 0°$) case, other than the instantaneous electronic response, $\langle \Delta n_p \rangle$ (noted as $\langle \Delta n_{p,\text{co}} \rangle$) shows multiple decay components with different decay constants. $\langle \Delta n_p \rangle$ keeps the same sign along the entire decay. The cross-polarized case, $\langle \Delta n_p \rangle$ ($\varphi = 90°$, $\langle n_{p,\text{cross}} \rangle$), first shows a weaker positive peak (i.e., the same sign as the copolarized case), followed by a dramatic decrease to a negative peak and then a slow decay. This is an indication of the influence of the reorientational nonlinearity that is stronger than the isotropic nonlinearity in CS_2. At delay times longer than 1 ps, where reorientational relaxation dominates, $\langle \Delta n_{p,\text{co}} \rangle = -2\langle \Delta n_{p,\text{cross}} \rangle$, consistent with the ratio calculated for a reorientational response. Both copolarized and cross-polarized response traces are very similar to the results obtained by the nonlinear interferometry technique, as described in Ref. [11]. Note that $\langle \Delta n_{\text{magic}} \rangle$ shows a response similar to the cross-correlation traces (not shown), with a slightly wider FWHM (by ~15%, accounting for GVM) which is probably due to a nuclear response with isotropic symmetry [21].

Based on Eqs. (11a) and (11c) and $\langle \Delta n_{\text{magic}} \rangle$, we can calculate $\langle \Delta n_{\text{iso}} \rangle$, and separate $\langle \Delta n_{\text{re}} \rangle$ from $\langle \Delta n_{\text{co}} \rangle$, shown as curves 4 and 5 in Fig. 3(b). While the quasi-instantaneous response of $\langle \Delta n_{\text{iso}} \rangle$ suggests a dominating

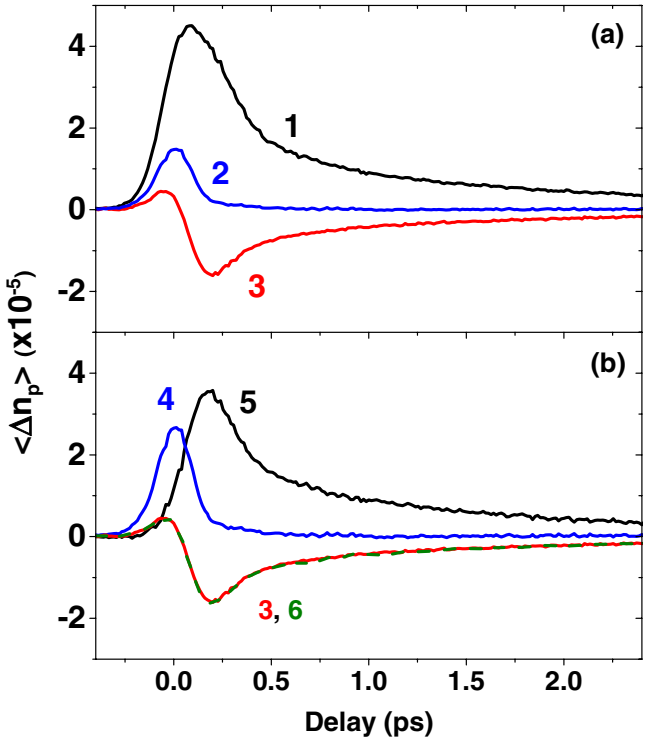

Fig. 3. (a) Averaged index change ($\langle \Delta n_p \rangle$) as a function of delay τ_d in CS_2 for (1) copolarized, (2) magic angle, and (3) cross-polarized cases with $L = 1$ mm, $\lambda_e = 800$ nm, $\lambda_p = 650$ nm, $w_e = 163$ μm, $w_{p,0} = 38$ μm, $\tau_e = 50$ fs, $\tau_p = 155$ fs, $I_{e,0} = 31$ GW/cm^2. (b) (4) isotropic nonlinear response ($\langle \Delta n_{\text{iso}} \rangle$), (5) and reorientational nonlinear response ($\langle \Delta n_{\text{re}} \rangle$) based on Eq. (11), and (6) reconstructed ($\langle \Delta n_p \rangle$) for cross-polarized case in comparison to direct experiment data (3). Note, curves 3 and 6 are essentially indistinguishable from each other.

bound-electronic nonlinearity with small isotropic nuclear response, the relatively slow response of $\langle \Delta n_{\text{re}} \rangle$ indicates a nonlinear contribution from purely nuclear motion. $\langle \Delta n_{\text{re}} \rangle$ rises and then shows a bi-exponential decay with a fast component of 180 fs and a slow component of 1.75 ps, respectively. The slow decay component originates from the reorientational relaxation, consistent with various literature data [3,11], the fast decay component is probably due to the libration of molecules [3], or the so-called intermolecular interaction-induced polarizability change [11], or a combination of both processes [9]. Note the results shown in Fig. 3 are similar to those measured by a dual-beam thermal lens method [10], but at a much lower noise level and higher temporal resolution. By using Eq (11b), we can use $\langle \Delta n_{\text{iso}} \rangle$ and $\langle \Delta n_{\text{re}} \rangle$ to reconstruct $\langle \Delta n_{p,\text{cross}} \rangle$ in the cross-polarized case, shown as curve 6 in Fig. 3(b) (note that curve 6 overlaps curve 3 in the figure). The precise agreement between the reconstructed curve and the experimental data unambiguously demonstrates the validity of using Eq. (11) to separate the different nonlinear mechanisms of CS_2 based on their tensor elements. We fit an n_2 for the isotropic response of $1.40 \pm 0.35 \times 10^{-15}$ cm^2/W ($1.83 \pm 0.45 \times 10^{-15}$ cm^2/W including GVM. [21]) This compares to estimates from Ref. [18] for the bound electronic n_2 of 2.9×10^{-15} cm^2/W as well as with our Z-scan results for ultrashort pulses of 2.5×10^{-15} cm^2/W [22].

In summary, we use a beam deflection technique, derived from photothermal deflection experiments, to measure the time and polarization dynamics of ultrafast NLR. The maximum sensitivity to induced phase change achieved was $\lambda/20,000$. By applying this technique to CS_2, we successfully separate the nonlinear response into its quasi-instantaneous isotropic nonlinearity and a much slower reorientational nonlinearity. The experimental results unambiguously agree with theoretical separation of these effects via their nonlinear susceptibility tensor elements. In the presence of NLA, the absorption gradient reshapes the irradiance profile to appear as though a lateral shift has occurred. Extension of this technique to materials with NLA will be discussed in a future publication.

This work is supported by AFOSR MURI grant FA9550-10-1-0558 and NSF grant ECCS1229563. We thank Zuo Wang and Kenji Kamada for useful discussions.

References and Note

1. M. Sheik-Bahae, A. A. Said, T.-H. Wei, D. J. Hagan, and E. W. Van Stryland, IEEE J. Quantum. Electron. **26**, 760 (1990).
2. R. A. Negres, J. M. Hales, A. Kobyakov, D. J. Hagan, and E. W. Van Stryland, IEEE J. Quantum Electron. **38**, 1205 (2002).
3. D. McMorrow, W. T. Lotshaw, and G. A. Kenney-Wallace, IEEE J. Quantum Electron. **24**, 443 (1988).
4. Q. Zhong and J. T. Fourkas, J. Phys. Chem. B **112**, 15529 (2008).
5. W. B. Jackson, N. M. Amer, A. C. Boccara, and D. Fournier, Appl. Opt. **20**, 1333 (1981).
6. J. D. Spear and R. E. Russo, J. Appl. Phys. **70**, 580 (1991).
7. G. P. Agrawal, Phys. Rev. Lett. **64**, 2487 (1990).
8. M. Sheik-Bahae, J. Wang, R. DeSalvo, D. J. Hagan, and E. W. V. Stryland, Opt. Lett. **17**, 258 (1992).
9. W. Li, L. Sarger, L. Canioni, P. Segonds, F. Adamietz, and A. Ducasse, Opt. Commun. **132**, 583 (1996).
10. M. Terazima, Opt. Lett. **20**, 25 (1995).
11. Y. Sato, R. Morita, and M. Yamashita, Jpn. J. Appl. Phys. **36**, 2109 (1997).
12. Y. H. Chen, S. Varma, I. Alexeev, and H. Milchberg, Opt. Express **15**, 7458 (2007).
13. P. Cong, Y. J. Chang, and J. D. Simon, J. Phys. Chem. **100**, 8613 (1996).
14. Y. J. Chang, P. Cong, and J. D. Simon, J. Chem. Phys. **106**, 8639 (1997).
15. J. A. Sell, D. M. Heffelfinger, P. L. G. Ventzek, and R. M. Gilgenbach, J. Appl. Phys. **69**, 1330 (1991).
16. L. W. Casperson, Appl. Opt. **12**, 2434 (1973).
17. D. N. Christodoulides, I. C. Khoo, G. J. Salamo, G. I. Stegeman, and E. W. Van Stryland, Adv. Opt. Photon. **2**, 60 (2010).
18. K. Kamada, Proc. SPIE **4797**, 65 (2003).
19. G. I. Stegeman and R. A. Stegeman, *Nonlinear Optics: Phenomena, Materials and Devices*, *Wiley Series in Pure and Applied Optics* (Wiley, 2012).
20. D. Milam, Appl. Opt. **37**, 546 (1998).
21. Subsequent to this work, analysis including GVM shows a small nuclear contribution with isotropic symmetry that gives an excellent fit to the cross-correlation data.
22. H. Hu, "Third order nonlinearity of organic molecules," Ph.D. dissertation (University of Central Florida, Orlando, FL, 2012).